Journal of Alloys and Compounds 853 (2021) 156700

Contents lists available at ScienceDirect

Journal of Alloys and Compounds

journal homepage: http://www.elsevier.com/locate/jalcom

Hollow carbon spheres loaded with uniform dispersion of copper oxide nanoparticles for anode in lithium- ion batteries

Martyna Trukawka [a], Karolina Wenelska [a, *], Lennart Singer [b], Rüdiger Klingeler [b, c], Xuecheng Chen [a, **], Ewa Mijowska [a]

[a] Faculty of Chemical Technology and Engineering, West Pomeranian University of Technology, Szczecin, Piastow Ave. 42, 71-065, Szczecin, Poland
[b] Kirchhoff Institute of Physics, Heidelberg University, INF 227, 69120, Heidelberg, Germany
[c] Centre for Advanced Materials (CAM), Heidelberg University, INF 225, 69120, Heidelberg, Germany

A R T I C L E I N F O

Article history:
Received 16 April 2020
Received in revised form
3 August 2020
Accepted 12 August 2020
Available online 11 September 2020

Keywords:
Hollow carbon spheres
Coper oxide
Spheres
Anode material
Lithium-ion batteries

A B S T R A C T

Lithium ion batteries are well established as a prominent option for electrical energy storage due to their high-power and high-energy density. Here, we demonstrate fully reversible conversion in hollow carbon spheres (HCSs) functionalized with copper oxide when applied as an anode material for lithium ion batteries. HCSs have been produced with hard template and glucose as a carbon precursor. Copper oxide has been prepared via thermal decomposition of copper precursor. The spherical structure is uniform in diameter of 160 nm and shell thickness of ~10 nm. Copper oxide (Cu_2O) nanoparticles of about 25 nm in diameter are homogeneously distributed inside HCSs. The carbon structure between Cu_2O nanoparticles buffers the volume change and prevents aggregation of Cu_2O nanoparticles. Clearly, it provides also unobstructed pathways for electron transport and Li^+ diffusion during charge/discharge processes. When evaluated as anode material for lithium ion batteries, HCSs with Cu_2O nanoparticles deliver an enhanced high specific capacity of 682 mAh/g at a current density of 50 mA/g and super stable cycling performances even at higher current rates in comparison with HCSs. Therefore, these findings reveal a great potential of HCS/Cu_2O nanoparticles as high-energy anode materials for LIBs.

1. Introduction

In recent years there is an ever-increasing demand for portable electronics for consumer as well as for professional applications which results in increasing energy demand of these devices. Currently, the dominant energy storage technology for portable electronic devices is rechargeable Li-ion batteries (LIBs), which is mainly due to their high energy density and superior rate performances but also because of their long cycling stability and low manufacturing cost compared to other secondary batteries[1-4]. However, the energy density of conventional graphite-based lithium ion battery cells is greatly limited because the stoichiometric limit of Li^+ intercalation restricts the theoretical capacitance of graphite to about 372 mAh/g (about 837 mAh/cm^3). Therefore, researchers are aiming at alternative high-capacitance anode materials. It seems that the carbon-based composite nanomaterials are well-suited for this purpose, since they increase the capacity of the anode even up to 1000 mAh/g[5]. A number of carbonaceous materials including graphene, nanotubes, fullerenes, nanosheets and nanofibers have been previously reported[6-17]. In most of the cited examples, high specific surface area and associated high reactivity with the electrolyte leads to ineffectiveness during the first cycle and the materials often suffer from severe capacity fading upon long-term cycling. A crucial parameter of electrode materials is its porosity. It is important in terms of material contact with the electrolyte solution which allows interfacial diffusion of Li ions, and thus determines the overall electrochemical efficiency. For this reason, it is considered that, the spherical morphology is advantageous for the electrode material as it facilitates homogeneous distribution of current, thereby reducing the electrolyte distribution and preventing growth of dendrites from lithium, i.e., improving the safety of LIBs. In the case of hollow carbon nanospheres (HCS) there is another advantage: the short diffusion distance for Li ions. It is also worth mentioning that the void space in the hollow particles can buffer against the volume change during Li

* Corresponding author.
** Corresponding author.
E-mail addresses: kwenelska@zut.edu.pl (K. Wenelska), xchen@zut.edu.pl (X. Chen).

https://doi.org/10.1016/j.jallcom.2020.156700
0925-8388/

ions insertion/desertion and thus achieve better electrochemical performance[18]. The above-mentioned properties of HCS can be used to create composites with transition metal oxides (TMO), because they have high theoretical capacities[19-22]. Especially, the use of only TMO as active material is hindered by their poor rate performance and low cycling life resulting from the large volume changes during the conversion processes as well as often limited transport of electrons and ions in the materials. Hence, when designing such carbon/TMO composite one should aim at rather small TMO nanoparticles in order to reduce the Li^+ diffusion distance[23-25]. Therefore, much work has been done to develop strategies that would alleviate these problems. One of them is combining TMO with carbon materials such as carbon nanotubes [26-29] or graphene[30-32] because carbon materials can enable fast electron transport, stabilize the system and act as elastic buffers.

Furthermore, there are many reports that the combination of carbonaceous material and copper oxide is characterized by high capacity and improved cyclability when used as anodes in LIBs. Liu *et al* published results for onion-like carbon coated Cu_2O nanocapsules which maintained a reversible capacity of 629 mAh/g after 50 cycles[33]. Zhang *et al* have reported Cu_2O nanowires/functionalized graphene composite. This material exhibited good cyclic stability and decent specific capacity of 677 mAh/g after 50 cycles [34]. There are also records reporting on other combinations of carbonaceous material and copper oxide such as nano-structured carbon-coated Cu_2O hollow spheres[35,36] mesoporous Cu_2O particles threaded with CNTs[37] or multi-yolk-shell copper oxide@carbon octahedral[38].

Herein, we report a facile and reproducible route to prepare HCSs functionalized by Cu_2O nanoparticles as advanced anode material for high performance LIBs as illustrated in Scheme 1. Hollow carbon spheres were obtained on a template of silica nanospheres using glucose as carbon source. Carbon structure between Cu_2O nanoparticles can buffer the volume change, preventing aggregation of the Cu_2O nanoparticles, and also providing unobstructed pathways for electron transport and Li^+ diffusion during charge/discharge processes. The electrochemical performance of HCS/Cu_2O was evaluated by cyclic voltammograms (CV) and galvanostatic charge-discharge (GCD). The results imply that HCS/Cu_2O electrodes possess large capacity, good capability and superior rate cycle stability.

2. Experimental section

2.1. Synthesis of SiO_2 sphere template

Silica spheres were prepared by the modified Stöber method. In a typical synthesis 4.5 mL of tetraethylorthosilicate (TEOS) was added to a mixture of ethanol (150 mL) and concentrated ammonia (25%, 6 mL). The solution was subsequently stirred for 16 h. Then, 0.45 mL of (3-Aminopropyl) triethoxysilane (APTES) was added and stirred for another 4 h. Finally, the product was dried in air at 90 °C for 24 h.

2.2. Synthesis of HCS

Above-prepared solid silica structures were used as a template to get HCSs. 0.5 g of silica spheres were dispersed in 80 mL of water. Then 0.5 g of glucose was added and stirred for 30 min. The mixture was placed in 100 mL autoclave at 180 °C for 12 h. In the next step, the product was separated by filtration, washed with ethanol, dried and annealed in inert gas at 800 °C for 2 h. Finally, to get HCS the product was washed with hydrofluoric acid to remove the silica.

2.3. Functionalization of HCS with copper oxide nanoparticles (HCS/Cu_2O)

The HCS modified by metal oxide nanoparticles (HCS/Cu_2O) were prepared according to the following procedure: 50 mg copper (II) sulfate were dispersed in 20 mL of ethanol and added dropwise to 50 mg of HCS while stirring and heating at 50 °C. Afterwards, the mixture was dried in air at 80 °C for 24 h. Then, the product was annealed in inert gas at 400 °C for 2 h.

2.4. Characterization

HR-TEM micrographs were collected using an FEI Tecnai G2 F20 S Twin with a field emission gun operating at 200 kV. The morphology of the samples was investigated by scanning electron microscopy (Hitachi SU8000), with an acceleration voltage of 30 kV. Raman scattering was conducted on a Renishaw micro-Raman spectrometer ($\lambda = 720$ nm). X-ray diffraction (XRD) was conducted on a Philips diffractometer (X'Pert PRO Philips diffractometer, Almelo, Holland) using Cu Kα radiation. The N_2 adsorption/desorption isotherms were acquired at liquid nitrogen temperature (77 K) via Micromeritics ASAP 2420 instrument, and the specific surface area was calculated by the Brunauer-Emmett-Teller (BET) method. The pore-size distribution (PSD) was determined by the Barret-Joner-Halenda (BJH) method. Thermogravimetric analysis (TGA) was carried out on 10 mg samples using a DTA-Q600 SDT TA at a heating rate of 10 C/min from room temperature to 900 °C under air.

2.5. Electrochemical measurements

The as-prepared HCS/Cu_2O nanomaterials were used as electrode materials for LIBs. The active materials, acetylene black and PVDF were mixed in a weight ratio of 85:10:5, respectively. Subsequently, *N*-methyl-pyrrolidone (NMP) was dropped to the powder in order to form a slurry. The working electrodes were fabricated by coating the slurry onto copper foam and dried in a vacuum at 80 °C overnight. The testing coin cells were assembled with the working electrode, metallic lithium foil as a counter

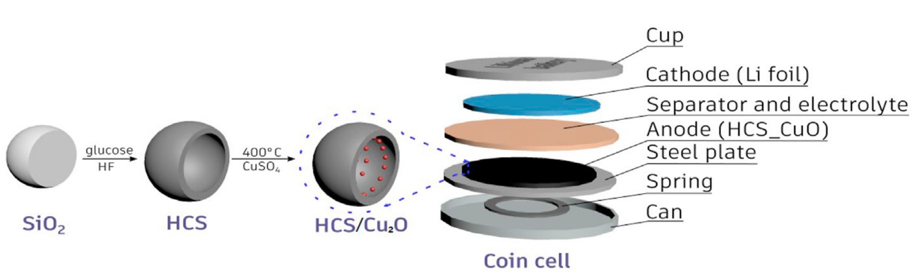

Scheme 1. Graphical illustration of HCS/Cu_2O synthesis route and coin cell composition.

electrode, NKK TK4350 film as separator, and 200 μl $LiPF_6$ in 1:1 ethylene carbonate (EC)/dimethyl carbonate (DMC) as the electrolyte. The assembly of the cells was carried out in an argon-filled glovebox (German, M. Braun Co.). Electrochemical studies were carried out by means of cyclic voltammetry (CV) and galvanostatic cycling with potential limitation (GCPL). The measurements were performed on a VMP3 multichannel potentiostat (BioLogic) at room temperature.

3. Results and discussion

Fig. 1 shows the XRD patterns of HCS/Cu_2O and HCS samples, respectively. In HCS, two broad diffraction peaks are observed at 24° and 44° which can be attributed to the (002) and (100) planes of graphitic carbon[39]. In addition to these broad features, several clear diffraction peaks in HCS/Cu_2O imply the presence of crystalline Cu_2O. Specifically, according to COD 1000063, diffraction peaks at 2θ values of 36.5, 42.5, 61.6, 73.8 and 77.6° can be assigned to the (111), (200), (220), (221), and (222) planes of cubic Cu_2O, respectively. The cubic lattice parameters of Cu_2O were calculated from the (111), (200), and (220) diffraction peaks using Bragg's law. The resulting value of $a = 4.252(2)$ Å agrees well with literature reports [40].

To further investigate the as-prepared samples, the morphology of the materials was studied by TEM and SEM (Fig. 2). Pristine hollow carbon nanospheres obtained from glucose on silica spheres template is shown in Fig. 2A. They are uniform in diameter of ~160 nm with the shells thickness ~10 nm. The size of copper oxide nanoparticles is in the range of 2–5 nm (see inset Fig. 2 D). SEM images indicated the maintaining of the spherical structure of the sample. Fig. 2C clearly shows that the surface of HCS/Cu_2O sample is smooth, demonstrating Cu_2O nanoparticles are supported inside of HCS instead of outside of HCS. No impurities or agglomerates were noticed. As discussed above, HR-TEM of the HCS/Cu_2O sample (Fig. 2D) shows only one kind of periodicity of lattice fringe with a spacing of 0.234 nm. This value nicely agrees to the separation of the (111) planes in Cu_2O as determined by XRD (see Fig. 1). Quantitatively, our XRD analysis yields 0.245(1) nm.

To further demonstrate the existence of Cu_2O nanoparticles supported in HCS, EDS mapping was used to characterize the prepared sample of HCS/Cu_2O. Fig. 3 presents the STEM image and EDS mapping of HCS/Cu_2O. It proves that Cu and O elements are evenly distributed in the sample of HCS/Cu_2O, further implying that Cu_2O nanoparticles have been successfully incorporated in HCS.

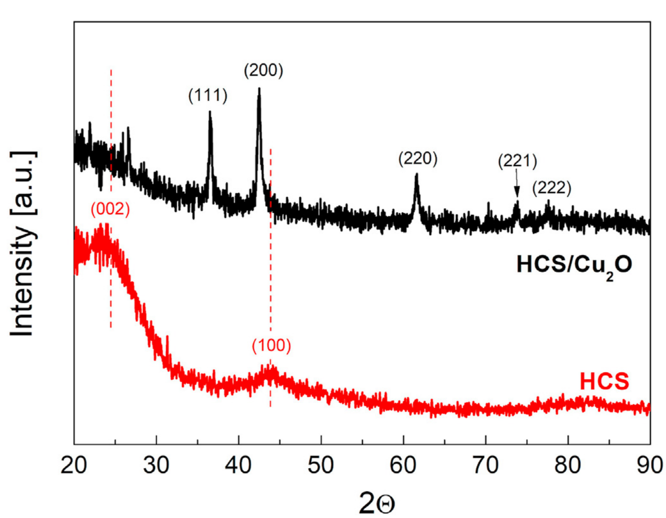

Fig. 1. XRD patterns of HCS (red) and HCS/Cu_2O (black). (For interpretation of the references to colour in this figure legend, the reader is referred to the Web version of this article.)

The N_2 adsorption/desorption measurements for HCS and HCS/Cu_2O shown in Fig. 4 imply typical type-IV profiles within relative pressure of 0–1, which suggests the presence of different pore sizes ranging from micro- to macropores. HCS exhibits larger specific surface area which decreases after modification with metal oxide nanoparticles. The parameter decrease upon Cu_2O functionalization indicates the presence of Cu_2O nanoparticles in the pores and their good distribution in the HCS. For HCS, the specific surface area is 1159 m^2/g with total a pore volume of 0.33 cm^3/g. After modification with Cu_2O nanoparticles, the specific surface area and the total pore volume decreased to 790 m^2/g and 0.18 cm^3/g, respectively (see Table 1).

Further information on the structure/defects of the materials is obtained by Raman spectroscopy (Fig. 5). The Raman spectra of the HCS and HCS/Cu_2O nanomaterials show two bands, i.e., the G- and D-band, which are characteristic for all graphitic materials. They are observed at ~1320 cm^{-1} (D) and ~1598 cm^{-1} (G). The G-band is associated with stretching of the C–C bond in graphitic materials which is common in all sp^2 carbon systems. The D-band is associated with the vibration of carbon atoms with dangling bonds in the plane with termination by disordered graphite. The intensity of the D-band measures the presence of such defects of the graphitic structure. To quantify disorder in carbon material, the I_D/I_G intensity ratio is estimated. The value of I_D/I_G for HCS/Cu_2O (~1.40) is not significantly higher than for HCS (~1.38), which may be associated with no changes in order of sp^2 bonded graphitic domains during decoration by Cu_2O nanoparticles[41].

The TGA measurements in Fig. 5 enable to reveal the carbon content and the quality of carbon nanospheres. Pristine HCS starts to decompose at 520 °C in air and the weight loss stops at 720 °C. This suggests that carbon spheres are less stable than pure graphite, which starts to burn above 600 °C[42]. There was no ash after combustion, which indicates high purity of HCS. TGA of HCS/Cu_2O reveals that the Cu_2O content is ~23 wt%. In addition, the data imply that the interaction of the metal oxide and the carbon induces lower stability of HCS. The main weight loss for HCS/Cu_2O starts at around 215 °C and ends at 400 °C.

3.1. Electrochemical measurements

To confirm the potential of the newly developed material (HCS/Cu_2O), lab-scale lithium cell prototypes were assembled using a HCS/Cu_2O-based electrode as anode. The cyclic performance of HCS/Cu_2O shows a variety of reversible redox reactions as well as irreversible processes, all of which governed by the electrochemical properties of both carbon and Cu_2O. Fig. 6A shows the initial discharge–charge curves from HCS/Cu_2O electrode in a half cell with a Li metal counter-electrode at the current density of 50 mAg^{-1}. In the reduction scan of the 1st cycle, the sample exhibits irreversible reactions at 0.6 V.

$$Cu_2O \cdot + \cdot 2Li^+ \cdot + \cdot 2e^- \cdot \rightarrow \cdot Cu \cdot + \cdot Li_2O \tag{1}$$

and the formation of solid electrolyte interface (SEI) at below 0.8 V. In this case the Cu_2O is reduced into Cu during the discharge process. In the oxidation scan, the decomposition of SEI occurred at below 2.0 V and the Cu metal is then re-oxidized into Cu_2O and partially into CuO at 2.0–2.7 V during the charge process.

$$2Cu \cdot + \cdot Li_2O \cdot \rightarrow \cdot Cu_2O \cdot + \cdot 2Li \cdot + \cdot Cuo \tag{2}$$

In the reduction region of the 2nd cycle, the CuO phase is reduced to Cu_2O at 2.4 V.

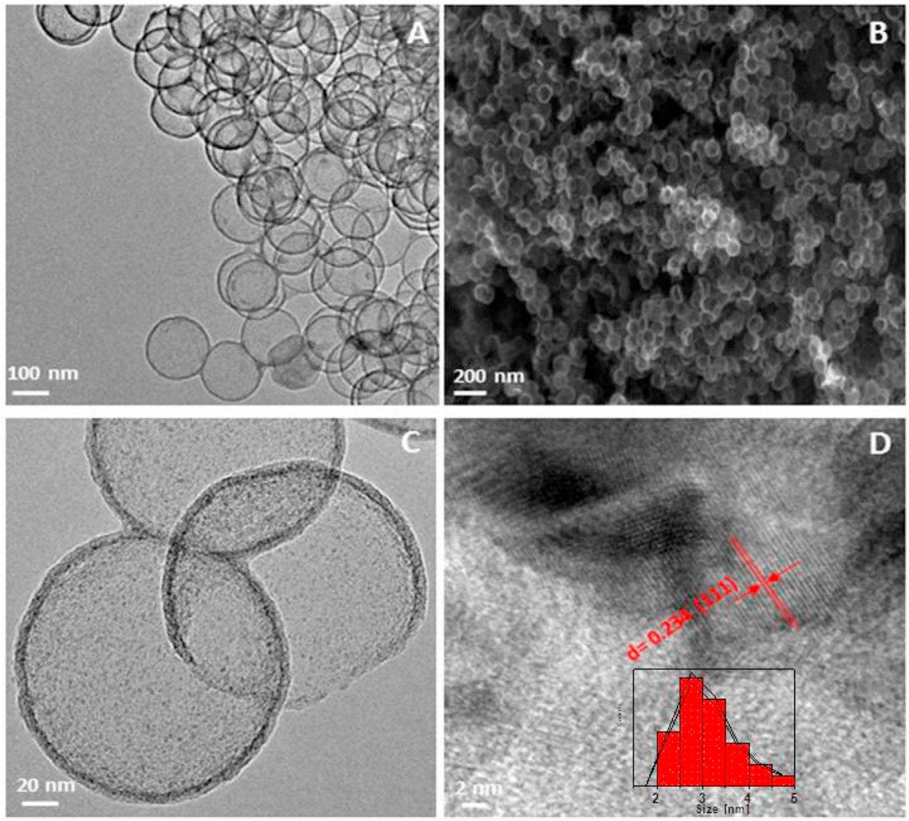

Fig. 2. (A) TEM images of HCS, (B) SEM, (C) TEM, (D) HRTEM images of HCS/Cu_2O, and Cu_2O nanoparticles size distribution as obtained from statistical analysis of the TEM images (inset).

$$Cuo\cdot + \cdot Li^{+}\cdot + \cdot e^{-}\cdot \rightarrow \cdot Cu_2O \tag{3}$$

and the Cu_2O phase is then reduced to the Cu metal at 1.4 V [43,44].

$$Cu_2O\cdot + \cdot 2Li^{+}\cdot + \cdot 2e\cdot \rightarrow \cdot Cu\cdot + \cdot Li_2O \tag{4}$$

Fig. 6B shows the first, the second and the fifth galvanostatic discharge−charge curves of the HCS/Cu_2O between 0.05 and 3.0 V (versus Li/Li+). The orange line shows the potential profile of the first charge and discharge cycle of HCS/Cu_2O (376 mA h g^{-1} and 860 mA h g^{-1}, respectively). The difference between the charge and discharge capacity in the first cycle can be assigned to irreversible effects such as the formation of the SEI layer. Thin SEI is formed on the HCS/Cu_2O electrode after cycling, and more mesopores are generated in the hollow structure, leading to the formation of interconnected spaces, which are favorable to fast transport of lithium ions and electrons. The stable SEI layer and hollow space on electrodes can stabilize lithiation/delithiation and mitigate the mechanical degradation originating from large volume expansion during discharge. The Cu_2O having dominant (111) facets, the enhanced of performance may be attributed to facilitating lithium ion transport during the discharging/ charging process. The capacity data in crystal planes of the Cu_2O play an important role in searching for high performance lithium-ion. The Cu_2O phase is easily oxidized to the CuO phase in this cell system. In addition, atom rearrangement and lattice/unit cell reconstruction were needed when the formation of monoclinic CuO from Cu2O phase occurred. However, on the (111) surfaces, which are a mixture of Cu and O atoms, it is difficult for the oxidation reaction to occur.

Multiple plateaus are clearly observed on both discharge/charge profiles, which are in good accordance with the CV curves. A sequential decay in reversible capacities as the rate increase can be observed. The electrode delivered capacities of 860 $mAhg^{-1}$, 487 $mAhg^{-1}$, 334 $mAhg^{-1}$, 219 $mAhg^{-1}$, 168 m hg^{-1} and 112 $mAhg^{-1}$ at current densities from 50 to 1000 mAg^{-1}. As shown in Fig. 6D, the new anode material exhibits good Li^+ storage capacity and cyclic stability at each current density from 50 to 1000 mA g^{-1}. Notably, the fused HCS/Cu_2O presents much higher capacities at each stage in comparison to pristine HCS[45]. Even at a very high current density of 1000 mAg^{-1}, a satisfying capacity value of ~112 $mAhg^{-1}$ is measured. It is interesting to note that even at a current density of 50 mAg^{-1} (second time), the capacity quickly returned to 590 $mAhg^{-1}$. These results indicate an excellent rate capability of the HCS/Cu_2O-based electrode.

The Cu_2O and its composites have been studied widely in LIBs and attained prominent achievements. The specific properties of Cu_2O and its composites for LIBs are given in Table 2. The ability of Cu_2O to retain its electrochemical capacity is significant and is strongly dependent on the second component of composite.

From the above results, it is confirmed that Cu_2O nanoparticles stored inside hollow carbon spheres exhibit excellent performance when used as anode material of lithium ion battery. Due to the synergistic effect between Cu_2O nanoparticles and hollow carbon spheres, the hybrid HCS/Cu_2O material shows enhanced capacities in which the void space in HCS can buffer against the volume change during Li^+ insertion/desertion.

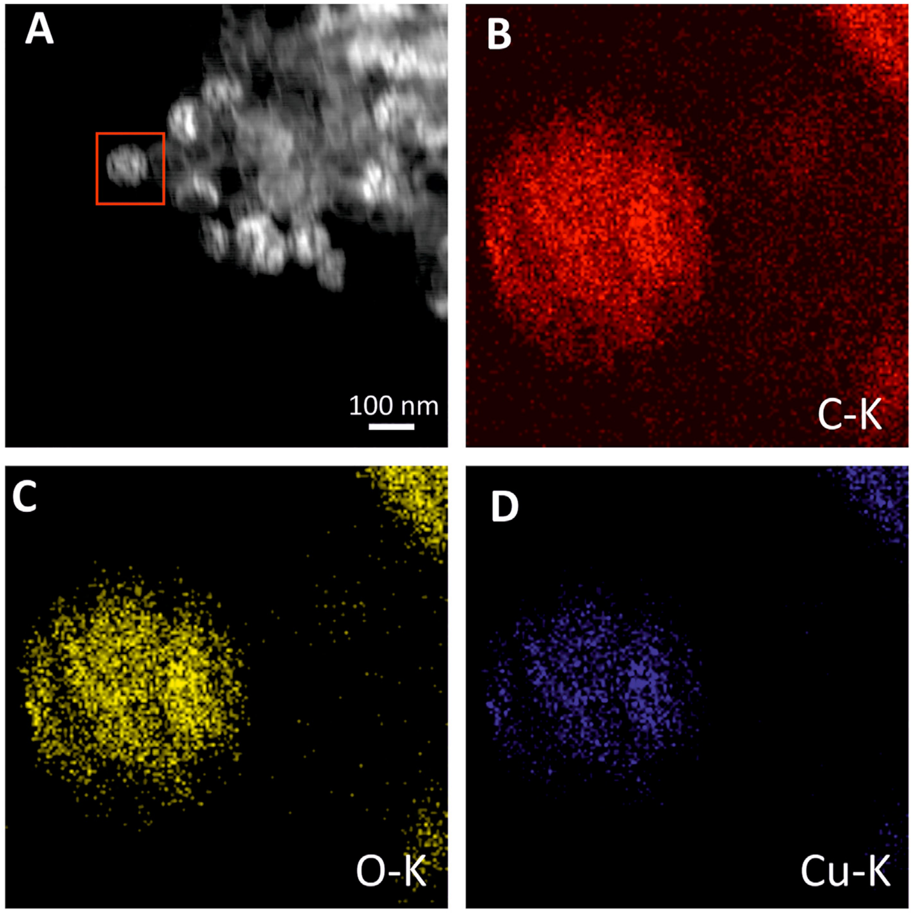

Fig. 3. (A) high-angle annular dark-field scanning transmission electron microscopy (STEM) and energy-dispersive X-ray spectroscopy (HAADF-STEM-EDS) mapping of (B) carbon, (C) oxygen, (D) copper of HCS/Cu_2O. The red square in (A) illustrates the region studied in (B) to (D). (For interpretation of the references to colour in this figure legend, the reader is referred to the Web version of this article.)

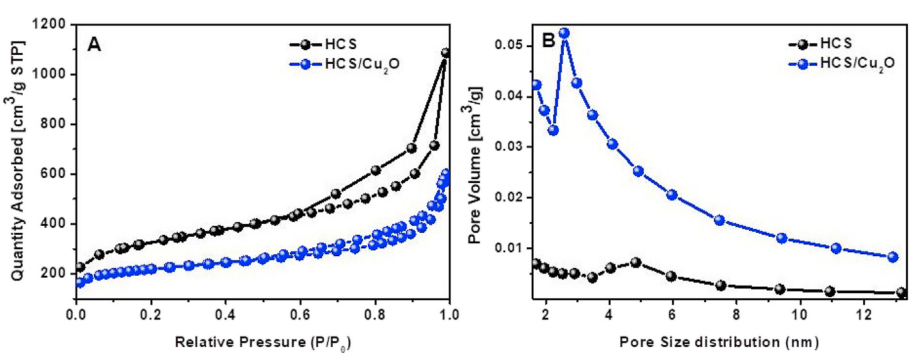

Fig. 4. N_2 adsorption/desorption isotherms (A) and pore size distribution profiles of HCS and HCS/Cu_2O.

Table 1
Specific surface area, total pore volume, and main pore size of HCS and HCS/Cu_2O as obtained by analysis of the N_2 adsorption/desorption isotherms in Fig. 4.

Sample	S_{BET} (m^2/g)	V_{TOTAL} (cm^3/g)	Pore Size (nm)
HCS	1159 ± 6.9	0.33	5.0
HCS/Cu_2O	791 ± 3.7	0.18	4.8

4. Conclusion

The contribution provides a facile route to prepare uniform hollow carbon nanospheres loaded with copper oxide nanoparticles. The spheres were obtained by the deposition of carbon from glucose onto silica sphere templates. Then, metal nanoparticles were selectively deposited inside HCS by precursor decomposition. The obtained HCSs were 160 nm in diameter with a shell thickness of about 10 nm. Based on TGA measurements, it was determined that the content of copper oxide was ~23 % wt. Also a slight decrease in order of sp^2 bonded graphitic domains with decoration of Cu_2O nanoparticles was noticed. High capacities and a good cycle performance make HCS/Cu_2O a promising anode material for rechargeable lithium ion batteries.

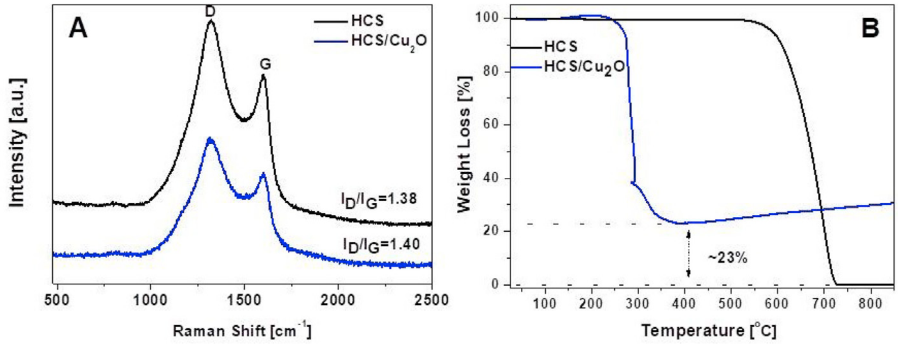

Fig. 5. (A) Raman spectroscopy and (B) TGA profile of HCS and HCS/Cu_2O.

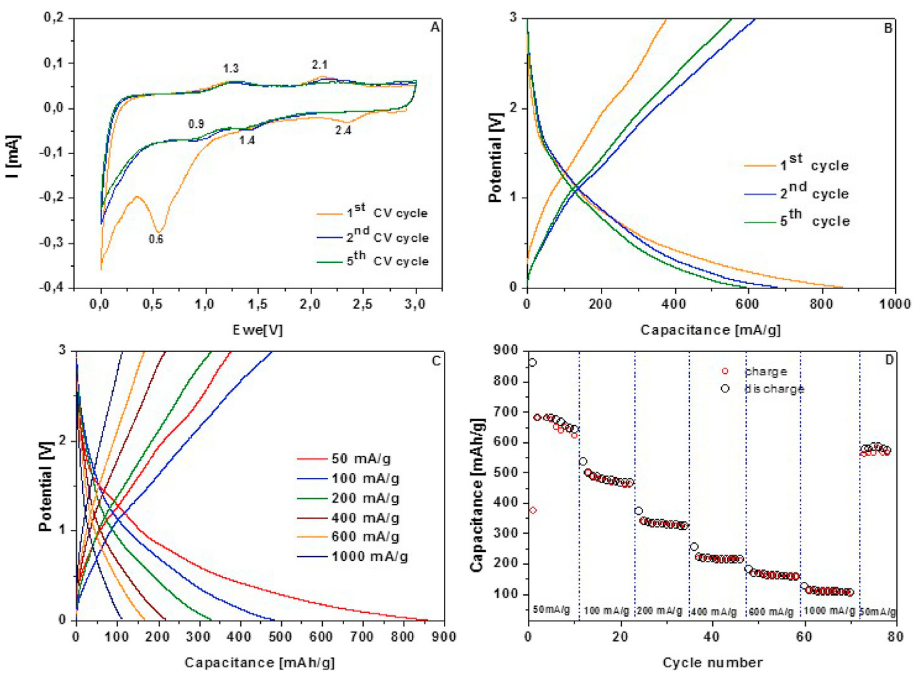

Fig. 6. (A) Cyclic voltammograms recorded over a potential window from 0.05 to 3 V at a scan rate from 0.5 mV s^{-1}, (B) galvanostatic charge/discharge profiles at a current density of 50 mA g^{-1} in the voltage range of 0.05–3.0 V, (C) voltage-capacity curves, (D) gravimetric specific capacities vs. cycle number of HCS/Cu_2O.

Table 2
Cu_2O and its composite materials for LIBs.

Materials	Disharge capacity [mAh g-1]	Ref.
Cu_2O/graphene hierarchical nanohybrids	857	[46]
Graphene oxide nanosheets Cu_2O	1326	[47]
Cu_2O/MXene	143	[48]
Cu_2O embedded in porous carbon	882.6	[49]
This work	**860**	
Core–shell structure morphology of Cu_2O 120 °C	351	[50]
Cubic shape Cu_2O	390	[51]

CRediT authorship contribution statement

Martyna Trukawka: Writing - original draft. **Karolina Wenelska:** Writing - original draft. **Lennart Singer:** Resources. **Rüdiger Klingeler:** Writing - review & editing. **Xuecheng Chen:** Conceptualization. **Ewa Mijowska:** Supervision.

Declaration of competing interest

The authors declare that they have no known competing financial interests or personal relationships that could have appeared to influence the work reported in this paper.

Acknowledgment

The authors acknowledge financial support from the National Science Centre, Poland, within Beethoven UMO-2016/23/G/ST5/04200 and by the Beethoven DFG project KL1824/12-1.

References

[1] J.B. Goodenough, Y. Kim, Challenges for rechargeable batteries, J. Power Sources 196 (2011) 6688–6694.
[2] V.G. Pol, M.M. Thackeray, Spherical carbon particles and carbon nanotubes prepared by autogenic reactions: evaluation as anodes in lithium electrochemical cells Energy, Environ. Sci. 4 (2011) 1904–1912.
[3] A. Manthiram, Materials challenges and opportunities of lithium ion batteries, J. Phys. Chem. Lett. 2 (2011) 176–184.
[4] S. Huang, J. Zhang, L. Yang, Ch Gong, J. Guo, P. Zhang, Q. Li, K. Huo, L. Mai, J. Yang, J. Zhang, Inward lithium-ion breathing of hollow carbon spheres-encapsulated Fe3O4@C nanodisc with superior lithium ion storage performance, J. Alloys Compd. (2019) 800.
[5] W. Wang, Z. Favors, C.L. Li, C. Liu, R. Ye, C.Y. Fu, K. Bozhilov, J.C. Guo, M. Ozkan, C.S. Ozkan, Silicon and carbon nanocomposite spheres with enhanced electrochemical performance for full cell lithium ion batteries, Sci. Rep. 7 (2017) 44838.
[6] L. Chen, Z. Wang, C. He, N. Zhao, C. Shi, E. Liu, A.J. Li, Uniform ultrasmall graphene oxide nanosheets with low cytotoxicity and high cellular uptake, ACS Appl. Mater. Interfaces 5 (2013) 9537–9545.
[7] R. Song, H. Song, J. Zhou, X. Chen, B. Wu, H.Y. Yang, Hierarchical porous carbon nanosheets and their favorable high-rate performance in lithium ion batteries, J. Mater. Chem. 22 (2012) 12369–12374.
[8] B.J. Landi, M.J. Ganter, C.D. Cress, R.A. Di Leo, R.P. Raffaelle, Carbon nanotubes for lithium ion batteries, Energy Environ. Sci. 2 (2009) 638–654.
[9] H.F. Xiang, Z.D. Li, K. Xie, J.Z. Jiang, J.J. Chen, P.C. Lian, J.S. Wu, Y. Yu, H.H. Wang, Graphene sheets as anode materials for Li-ion batteries: preparation, structure, electrochemical properties and mechanism for lithium storage, RSC Adv. 2 (2012) 6792–6799.
[10] D. Bhattacharjya, H.Y. Park, M.S. Kim, H.S. Choi, S.N. Inamdar, J.S. Yu, Nitrogen-Doped carbon nanoparticles by flame synthesis as anode material for rechargeable lithium-ion batteries, Langmuir 30 (2014) 318–324.
[11] W. Sun, Y. Wang, Graphene-based nanocomposite anodes for lithium-ion batteries, Nanoscale 6 (2014) 11528–11552.
[12] Z. Li, A. Ottmann, Q. Sun, A.K. Kast, T. Zhang, H.-P. Meyer, C. Backes, R. Schröder, J. Xiang, Y. Vaynzof, R. Klingeler, Hierarchical MoS_2-carbon porous nanorods towards atomic interfacial engineering for high-performance lithium storage, J. Phys. Chem. 7 (2019) 7553–7564.
[13] E. Thauer, A. Ottmann, P. Schneider, L. Möller, L. Deeg, R. Zeus, F. Wilhelmi, L. Schlestein, C. Neef, R. Ghunaim, et al., Molecules 25 (2020) 1064.
[14] G. Wang, J. Deng, T. Yan, J. Zhang, L. Shi, D. Zhang, Turning on electrocatalytic oxygen reduction by creating robust Fe–Nx species in hollow carbon frameworks via in situ growth of Fe doped ZIFs on g-C3N4, Nanoscale 12 (2020) 5601–5611.
[15] J. Zhang, J. Fang, J. Han, T. Yan, L. Shi, D. Zhang, P. N, S co-doped hollow carbon polyhedra derived from MOF-based core–shell nanocomposites for capacitive deionization, J. Mater. Chem. 6 (2018) 15245–15252.
[16] P. Liu, Y. Liu, J. Jiang, S. Ashraf, X. Wu, G. Han, J. Gao, K. Zhang, B. Li, Co-, Fe-, and N-modified carbon composites for excellent catalytic performances toward electrochemical reduction reaction, ACS Sustain. Chem. Eng. 7 (9) (2019) 8744–8754.
[17] L. Yan, D. Li, T. Yan, G. Chen, L. Shi, Zhongxun an, D. ZhangN,P,S-Codoped hierarchically porous carbon spheres with well-balanced gravimetric/volumetric capacitance for supercapacitors, ACS Sustain. Chem. Eng. 6 (4) (2018) 5265–5272.
[18] V. Etacheri, C. Wang, M.J. O'Connell, C.K. Chan, V.G. Pol, Porous carbon sphere anodes for enhanced lithium-ion storage, J. Mater. Chem. 3 (2015) 9861–9868.
[19] S. Hao, B. Zhang, S. Ball, B. Hu, J. Wu, Y. Huang, Porous and hollow NiO microspheres for high capacity and long-life anode materials of Li-ion batteries Mater, DES 92 (2016) 160–165.
[20] X. Qian, Q. Xu, T. Hang, S. Shanmugam, M. Li, Electrochemical deposition of Fe_3O_4 nanoparticles and flower-like hierarchical porous nanoflakes on 3D Cu-cone arrays for rechargeable lithium battery anodes Mater, DES 121 (2017) 321–334.
[21] S.Z. Huang, J. Jin, Y. Cai, Y. Li, H.Y. Tan, H.E. Wang, G. Van Tendeloo, B.-L. Su, Engineering single crystalline Mn_3O_4 nano-octahedra with exposed highly active {011} facets for high performance lithium ion batteries, Nanoscale 6 (2014) 6819–6827.
[22] H. Yuan, J. Li, W. Yang, Z. Zhuang, Y. Zhao, L. He, L. Xu, X. Liao, R. Zhu, L. Mai, Oxygen vacancy-determined highly efficient oxygen reduction in NiCo2O4/hollow carbon spheres, ACS Appl. Mater. Interfaces 10 (19) (2018) 16410–16417.
[23] S. Zhu, J.J. Li, X.Y. Deng, C. He, E.Z. Liu, F. He, C. Shi, N. Zhao, Ultrathin-nanosheet-induced synthesis of 3D transition metal oxides networks for lithium ion battery anodes, Adv. Funct. Mater. 27 (2017) 1605017.
[24] P. Poizot, S. Laruelle, S. Grugeon, L. Dupont, J.-M. Tarascon, Nano-sized transition-metal oxides as negative-electrode materials for lithium-ion batteries, Nature 407 (2000) 496–499.
[25] L. Martin, H. Martinez, D. Poinot, B. Pecquenard, F. Le Cras, Direct observation of important morphology and composition changes at the surface of the Cu_2O conversion material in lithium batteries, J. Power Sources 248 (2014) 861–873.
[26] X. Cui, Y. Wang, Z. Chen, H. Zhou, Q. Xu, P. Sun, J. Zhou, L. Xia, Y. Sun, Y. Lu, Preparation of pompon-like MnO/carbon nanotube composite microspheres as anodes for lithium ion batteries Electrochim, Acta 180 (2015) 858–865.
[27] R. Wu, D.P. Wang, X. Rui, B. Liu, K. Zhou, A.W.K. Law, Q. Yan, J. Wei, Z. Chen, In-Situ formation of hollow hybrids composed of cobalt sulfides embedded within porous carbon polyhedra/carbon nanotubes for high-performance lithium-ion batteries, Adv. Mater. 27 (2015) 3038–3044.
[28] X. Cui, Y.Q. Wang, Q.Y. Xu, P.P. Sun, X.Z. Wang, T. Wei, Y.M. Sun, Carbon nanotube entangled Mn_3O_4 octahedron as anode materials for lithium-ion batteries, Nanotechnology 28 (2017) 255402.
[29] A. Ottmann, M. Scholz, M. Haft, E. Thauer, P. Schneider, M. Gellesch, C. Nowka, S. Wurmehl, S. Hampel, R. Klingeler, Electrochemical magnetization switching and energy storage in manganese oxide filled carbon nanotubes, Sci. Rep. 7 (2017) 13625.
[30] B. Rangasamy, J.Y. Hwang, W. Choi, Multi layered Si-Cu_2O quantum dots wrapped by graphene for high-performance anode material in lithium-ion battery, Carbon 77 (2014) 1065–1072.
[31] G.D. Park, Y. Kang, Superior lithium-ion storage properties of mesoporous Cu_2O–reduced graphene oxide composite powder prepared by a two-step spray-drying process, Chem. Eur J. 21 (2015) 9179–9184.
[32] J. Xu, J. Wu, L. Luo, X. Chen, H. Qin, V. Dravid, S. Mi, C. Jia, Co_3O_4 nanocubes homogeneously assembled on few-layer graphene for high energy density lithium-ion batteries, J. Power Sources 274 (2015) 816–822.
[33] X. Liu, N. Bi, C. Feng, S.W. Or, Y. Sun, C. Jin, W. Li, F. Xiao, Onion-like carbon coated Cu_2O nanocapsules: a highly reversible anode material for lithium ion batteries, J. Alloys Compd. 587 (2014) 1–5.
[34] J. Zhang, B. Wang, J. Zhou, R. Xia, Y. Chu, J. Huang, Preparation of advanced Cu_2O nanowires/functionalized graphene composite anode material for lithium ion batteries, Materials 10 (2017) 72.
[35] Y. Xu, G. Jian, M.R. Zachariah, C. Wang, Nano-structured carbon-coated Cu_2O hollow spheres as stable and high rate anodes for lithium-ion batteries, J. Mater. Chem. 1 (2013) 15486.
[36] Z. Deng, Y. Li, Z. Ma, J. Zhao, J. Cao, D. Zhang, Facile one-pot synthesis of hollow Cu2O spheres with porous shells as high-performance anode materials for lithium ion batteries, Curr. Nanosci. 11 (4) (2015) 470–474.
[37] S. Ko, J.-I. Lee, H.S. Yang, S. Park, U. Jeong, Mesoporous Cu_2O particles threaded with CNTs for high-performance lithium-ion battery anodes, Adv. Mater. 24 (2012) 4451–4456.
[38] T. Chen, Y. Hu, B. Cheng, R. Chen, H. Lv, L. Ma, G. Zhu, Y. Wang, C. Yan, Z. Tie, Z. Jin, J. Liu, Multi-yolk-shell copper oxide@carbon octahedra as high-stability anodes for lithium-ion batteries, Nano Energy 20 (2016) 305–314.
[39] Y. Lu, X. Wen, X. Chen, P.K. Chu, T. Tang, E. Mijowska, Nitrogen-Doped porous carbon embedded with cobalt nanoparticles for excellent oxygen reduction reaction, J. Colloid Interface Sci. 546 (2019) 344–350.
[40] M.C. Neuburger, Präzisionsmessung der Gitterkonstante von Cuprooxyd Cu_2O, Z. Phys. 67 (1931) 11–12.
[41] S. Mildred, A.J. Dresselhaus, H. Mario, D. Gene, S. Riichiro, Perspectives on carbon nanotubes and graphene Raman spectroscopy, Nano Lett. 10 (2010) 751–758.
[42] Y. Devrim, A. Albostan, Graphene-supported platinum catalyst-based membrane electrode assembly for PEM fuel cell, J. Electron. Mater. 45 (2016) 8.
[43] X. Zhang, L. Yu, L. Wang, R. Ji, G. Wang, B. Geng, High electrochemical performance based on ultrathin porous CuO nanobelts grown on Cu substrate as integrated electrode, Chem. Phys. 15 (2013) 521–525.
[44] C.Q. Zhang, J.P. Tu, X.H. Huang, Y.F. Yuan, X.T. Chen, F. Mao, Preparation and electrochemical performances of cubic shape Cu_2O as anode material for lithium ion batteries, J. Alloys Compd. 441 (2007) 52–56.
[45] X. Shi, S. Zhang, X. Chen, T. Tang, R. Klingeler, E. Mijowska, Ultrathin NiO confined within hollow carbon sphere for efficient electrochemical energy storage, J. Alloys Compd. 797 (2019) 702–709.
[46] Y. Zhang, X. Wang, L. Zeng, S. Song, D. Liu, Green and controlled synthesis of Cu2O–graphene hierarchical nanohybrids as high-performance anode materials for lithium-ion batteries via an ultrasound assisted approach, Dalton Trans. 41 (2012) 4316.
[47] Y. Xu, Y. Guo, C. Li, X. Zhou, M.C. Tucker, X. Fu, R. Sun, C. Wong, Enhanced performance of lithium-ion batteries with copper oxide microspheres @ graphene oxide micro/nanocomposite electrodes, Nano Energy 11 (2015) 38.
[48] H. Zhang, H. Dong, X. Zhang, Y. Xu, J. Fransaer, Cu2O hybridized titanium carbide with open conductive frameworks for lithium-ion batteries, Electrochim. Acta 202 (2016) 24.
[49] X. Shen, S. Chen, D. Mu, B. Wu, F. Wu, Novel synthesis and electrochemical performance of nano-structured composite with Cu2O embedment in porous carbon as anode material for lithium ion batteries, J. Power Sources 238 (2013) 173.
[50] L.J. Fu, J. Gao, T. Zhang, Q. Cao, L.C. Yang, Y.P. Wu, R. Holze, H.Q. Wu, Preparation of Cu2O particles with different morphologies and their application in lithium ion batteries, J. Power Sources 174 (2007) 1197.
[51] C.Q. Zhang, J.P. Tu, X.H. Huang, Y.F. Yuan, X.T. Chen, F. Mao, Preparation and electrochemical performances of cubic shape Cu2O as anode material for lithium ion batteries, J. Alloys Compd. 441 (2007) 52.